Available online at www.sciencedirect.com
ScienceDirect
Catalysis Today 131 (2008) 219–225
CATALYSIS TODAY
www.elsevier.com/locate/cattod

Preparation and application of mesocellular carbon foams to catalyst support in methanol electro-oxidation

Ji Bong Joo [a], Pil Kim [b], Wooyoung Kim [a], Jongheop Yi [a,*]

[a] School of Chemical and Biological Engineering, Institute of Chemical Processes, Seoul National University, Shinlim-dong, Kwanak-ku, Seoul 151-742, South Korea
[b] School of Environmental and Chemical Engineering, Chonbuk National University, Deokjin-dong 1 ga, Deokjin-gu, Jeonju, Jeonbuk 576-756, South Korea

Available online 28 November 2007

Abstract

A novel and simple preparation method for preparing a mesocellular carbon foam (MCF-C) is described. A silica–polymer composite as an amphi-templating material was synthesized by a sol–gel method using tetraethyoxy-orthosilicate (TEOS), P123 and divinylbezene (DVB) as a silica precursor, a template and a polymer precursor, respectively. The silica–polymer composite was subsequently transformed to either mesocellular carbon foam (MCF-C) or mesocellular silica foam (MCF-S). The prepared MCF-C exhibited well-developed mesocell pore structures with uniform windows. Compared to conventional methods, the method used for preparing MCF-C was economical and simple. MCF-C was used as a catalyst support in methanol electro-oxidation. The Pt/MCF-C-ETX (MCF-C-supported Pt catalyst which was prepared using sodium ethoxide) catalyst has smaller Pt nanoparticles and a larger electrochemically active surface area (EAS) value than the commercial Pt/C catalyst. In methanol electro-oxidation, the prepared Pt/MCF-C-ETX catalyst showed a higher catalytic performance than the commercial Pt/C catalyst.

Keywords: Mesocellular carbon foam; Silica–polymer composite; Catalyst; Methanol; Fuel cells

1. Introduction

Since the discovery of M41s by mobile researchers, mesoporous materials have attracted tremendous attentions for their possible application in areas such as nanocomposites, quantum electronic devices, electrode materials and catalysts [1–4]. Ordered mesoporous materials such as M41s, SBA-*x* and CMK-*x* are typically synthesized by a self-assembly templating method or an inverse replica templating method using a nano-structured organic or an inorganic template [5,6]. However, these kinds of mesoporous materials have a limited pore range of 2–5 nm. For reactions involving bulky molecules, a larger pore is required to minimize the diffusion resistance of reactants. For the above reasons, several research groups have synthesized mesoporous silica materials with large pores [7–11].

Other mesoporous materials with large pores such as mesocellular polymers, mesocelluar carbons and other disordered porous materials can be synthesized using silica templates [12,13]. In addition, mesoporous materials, which have larger pore over 10 nm, can be produced by inverse replication using silica nano particles. For example, mesocellular polymer foam was successfully synthesized using a mesocellular silica foam by Hyeon and co-workers [12]. In some cases, the spherical silica and polymer particles have been used as a template for preparing mesocellular carbon foams (MCF-C) [14,15].

Mesoporous carbon materials were usually used as electro-catalyst supports and electrode materials in electrochemical systems due to their unique characteristics which include high surface areas and electro-conductivities [16–19]. Ryoo and co-workers reported the synthesis of mesoporous carbon CMK-5 using SBA-15, which exhibited the enhanced electro-catalytic activity in the oxygen electro-reduction [19]. However, small pores size (below 10 nm) would not be suitable in practical fuel cell environment because the bulky ionomer could not be easily distributed in small pores of carbon support. For the high performance in fuel cell, mesoporous carbons, which have favorable pore structure and large pore, are required.

In this study, we report a novel method for the preparation of both MCF-C and MCF-S using a silica–polymer composite as

* Corresponding author. Tel.: +82 2 880 7438; fax: +82 2 885 6670.
E-mail address: jyi@snu.ac.kr (J. Yi).

0920-5861/$ – see front matter
doi:10.1016/j.cattod.2007.10.086

amphi-templating material. The intermediate silica–polymer composite was easily transformed to either MCF-S or MCF-C by a subsequent process such as calcination or carbonization. Compared to the conventional preparation method for MCF-C, the synthetic process employed in this work is a simple and an efficient method. The prepared MCF-C support was used as the catalyst support for a Pt catalyst in methanol electro-oxidation.

2. Experimental

2.1. Preparation of MCF-S and MCF-C

The silica–polymer composite was prepared by a typical sol–gel method. Pluoric P123 (EO_{20}-PO_{70}-EO_{20}, M_{av} = 5800, BASF) a triblock copolymer and tetraethyoxy-orthosilicate (TEOS, Fluka) were used as a template and a silica precursor, respectively. Divinylbenzene (DVB, Aldrich) was used as a polymer precursor. In a typical procedure, P123 was dissolved in an aqueous HCl solution at room temperature. After the P123 was completely dissolved in the solution, the DVB was added to the above solution under vigorous stirring. When the DVB was well dissolved, TEOS was added to the solution. After stirring of the above solution for 12 h at 40 °C, azobisisobutyronitrile (AIBN, Aldrich) was added to the mixture. The final composition of the mixture employed in this work was P123 (1): TEOS (40): DVB (7.5): AIBN (0.375). The resulting mixture was stirred for 12 h and then aged for 24 h at 80 °C, to give precipitate of a light yellow silica–polymer composite. The precipitate was filtered and dried at 80 °C. MCF-C was obtained by carbonization of the silica–polymer composite, followed by selective silica etching using a dilute HF solution.

2.2. Preparation of MCF-C-supported Pt catalysts

The MCF-C-supported Pt catalyst was prepared by a reported method [20]. Briefly, H_2PtCl_6 (Acrose) and sodium ethoxide (Aldirich, $NaOCH_2CH_3$) were dissolved in ethanol. The MCF-C was well dispersed into the above ethanolic solution and the mixture was sonicated for 20 min. The resulting mixture was stirred at 60 °C for the complete reduction of Pt ions. After the reduction of Pt ions for 6 h, a dilute HCl solution was added to the mixture to deposit the reduced Pt nanoparticles on MCF-C. The resulting black precipitate was filtered, washed by copious amount of de-ionized water and dried at 120 °C, to give Pt/MCF-C-ETX. The total Pt loading was adjusted to 60 wt.% in the final catalyst. For the purpose of comparison, a Pt catalyst was prepared using $NaBH_4$ as a reducing agent and a Vulcan XC-72 carbon black as a support (Pt/C-$NaBH_4$). In the preparation, the carbon support and Pt precursor were homogeneously mixed, followed by reduction of the Pt precursor with a 0.2 M $NaBH_4$ solution.

2.3. Characterization

N_2 adsorption isotherms of the prepared carbon were obtained at 77 K using a nitrogen sorption instrument (Micromeritics ASAP 2010). Pore size distributions were calculated by the BJH method. Crystalline phases of the prepared Pt catalysts were investigated by X-ray diffraction using Cu Kα radiation (MAC science M18XHF-SRA). Pore sizes and macroscopic morphologies of the carbon supports and the supported Pt catalysts were observed by transmission electron microscopy (TEM, Jeol JEM-2000EXII).

2.4. Electrochemical characterization and half cell tests

The electrochemically active surface areas (EAS) of the prepared catalysts were measured by cyclic voltammetry using an EG&G 263A potentiostat. Cyclic voltammograms (CVs) of the supported Pt catalyst were measured using a conventional three-electrode system with a saturated calomel electrode (SCE) and a platinum gauge as a reference electrode and a counter electrode, respectively. The working electrode was prepared by coating catalyst ink on disk-type graphite. The CVs were obtained at room temperature at a scan rate 20 mV/s in a 0.5 M H_2SO_4 solution from −0.25 to 1.0 V versus SCE. In order to investigate the catalytic activity in electro-oxidation of methanol, CVs were obtained in a 0.5 M H_2SO_4 solution containing 2 M CH_3OH.

For CO stripping voltammograms, CO was adsorbed to the Pt catalyst by bubbling CO in the electrolyte of 0.5 M H_2SO_4 for 30 min, while holding the working electrode potential at 0.1 V versus the RHE (reversible hydrogen electrode). After CO bubbling, the gas was switched to nitrogen for 20 min and the potential was scanned from −0.25 to 1.0 V versus SCE to record CO stripping voltammograms.

3. Results and discussion

3.1. Characteristics of MCFs

Fig. 1 shows the procedure used to prepare the mesocelluar carbon foam. As shown in Fig. 1(a), it is generally known that MCF-S was firstly synthesized using an organic template and swelling agent such as trimethylbenzene (TMB). After the preparation of MCF-S, the carbon precursor was impregnated into the pores of the MCF-S and a replica MCF-C was then synthesized by subsequent treatments such as carbonization and selective silica etching. Since this preparation process involves numerous steps, it is time-consuming and inefficient process for preparing MCF-C. However, we propose herein a simple and novel method for preparing of MCF-C (Fig. 1(b)).

In this work, DVB monomer was used both as a swelling agent and a carbon precursor. In the conventional MCF synthesis, TMB has been used as a swelling agent and is believed to be preferentially soluble in the hydrophobic core of the micelle (Fig. 2(a)). However, it would be expected that DVB would exhibit different behavior. It should be noted that DVB has relatively less hydrophobic vinyl functional group compared to TMB and shows the amphiphilic properties in micelles. Thus, DVB is distributed in the less hydrophobic phase of the PEO group as shown in Fig. 2(b). DVB molecules are then mixed with silica precursors. After the condensation of TEOS, DVB monomers are located in complementary pores of

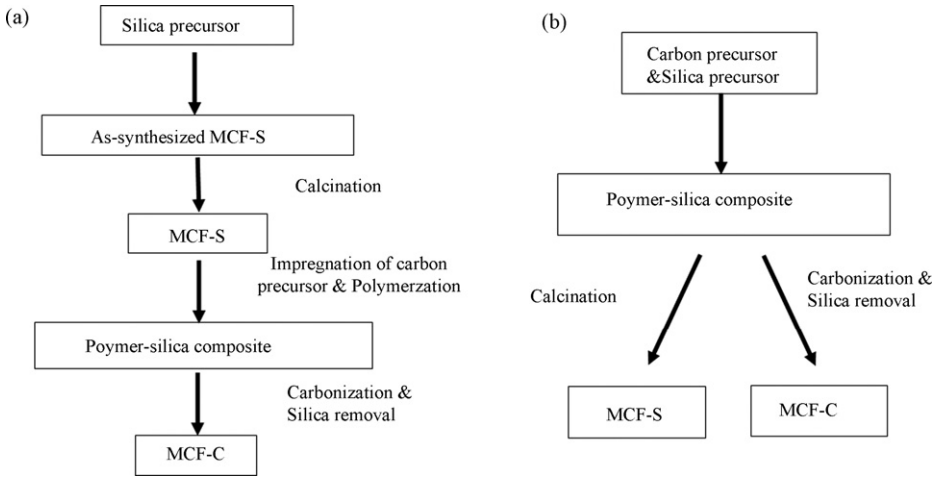

Fig. 1. Preparation procedure for MCF-C: (a) conventional method and (b) the suggested method.

silica structure outside of micelles [12,13]. After the polymerization of DVB, the complementary pores would be filled with polymer (polydivinylbenzene).

The N_2 adsorption–desorption isotherm and pore size distributions of MCF-C are shown in Fig. 3. As shown in Fig. 3(a), MCF-C has a typical type IV isotherm and well developed H1 hysteresis loop with dramatic adsorption and desorption at a high relative pressure (ca. 0.8–0.9), indicating mesoporous characteristics with large cells and window pores. Pore diameters of the main cell pore and windows were determined from the adsorption and desorption branches of the nitrogen isotherms. Two sharp peaks were observed in the pore size distribution indicating both uniform sized cells (ca. 30 nm) and windows (ca. 18 nm) (Fig. 2(b)). The BET surface area and total pore volume of MCF-C were 810 m^2/g and 2.40 cm^3/g.

TEM image of MCF-C is shown in Fig. 4. MCF-C shows well-defined spherical cell pores with a uniform size. The cell pore sizes estimated from TEM images are in good agreement with the results of the N_2 adsorption analyses.

3.2. Characteristics and electro-catalytic activities of the supported Pt catalysts

To identify the crystalline phase of Pt catalysts employed in this work, an X-ray diffraction technique was applied. Fig. 5 exhibits XRD patterns of the supported Pt catalysts. As shown in Fig. 5, typical characteristic peaks for Pt (1 1 1), Pt (2 2 0) and Pt (2 0 0) were observed on ca. 39°, 46° and 68° in all the supported Pt catalysts. These results indicate that a face-centered cubic (fcc) structure of Pt was formed on the supported Pt catalysts. The

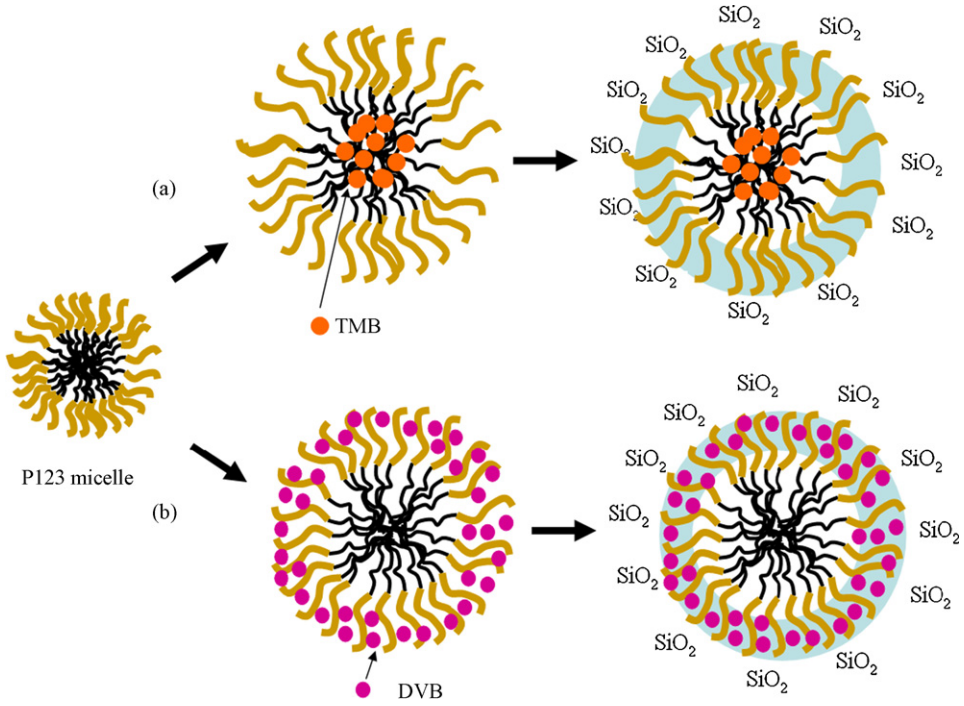

Fig. 2. Synthesis schematics for MCF using each swelling agent: (a) TMB and (b) DVB.

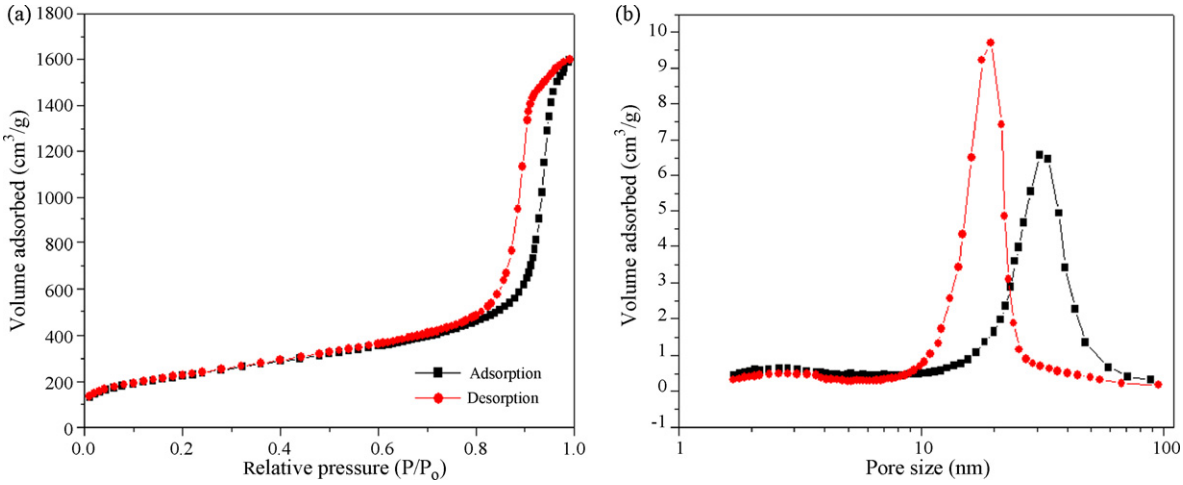

Fig. 3. N_2 adsorption–desorption isotherms and pore size distributions of (a) MCF-C and (b) MCF-S.

Pt/MCF-C-ETX exhibited the broadest diffraction peaks among the supported Pt catalysts, indicating the smallest Pt crystallites. Excepted for the Pt/MCF-C-ETX catalyst, the two catalysts showed similar peak broadness, indicating that the sizes of the Pt crystallites were almost identical.

The average crystalline size of Pt was calculated using the Scherrer equation based on the Pt (2 2 0) diffraction peaks, because the Pt (2 2 0) peak is isolated from the other diffraction peaks such as carbon and other metal [21,22]. The surface areas of Pt were estimated from the Pt crystalline sizes using the following equation: $S = 6000/\rho d$, where d is average crystallite size (nm), S is the surface area (m^2/g), and ρ represents Pt density (21.4 g/cm^3). The crystalline sizes and surface areas of Pt are listed in Table 1. Pt/MCF-C-ETX showed the smallest Pt crystalline size and the highest surface area among the supported Pt catalysts.

Fig. 6 shows TEM images of the prepared Pt catalysts. As shown in Fig. 6(c), it can be easily observed that the uniform-sized Pt nano-particles are highly dispersed on the MCF-C. Compared to other Pt catalysts, Pt/MCF-C-ETX exhibits a high metal dispersion and a small size of Pt. On the other hand, the two Pt catalysts showed similar characteristics and metal dispersion. Pt/C-commercial and Pt/C-$NaBH_4$ exhibited that Pt nano-particles were dispersed on spherical carbon particles and some of Pt nano-particles were aggregated. The Pt sizes of Pt/MCF-C-ETX, Pt/C-commercial and Pt/C-$NaBH_4$ were estimated to be ca. 2.7, 4.8 and 5.0 nm, well consistent with XRD results.

Fig. 7 shows CVs of the supported Pt catalysts under acidic conditions (0.5 M H_2SO_4), which were used to estimate the EAS using the coulombic charge for proton ion adsorption–desorption. The CVs of the supported Pt catalysts exhibit a typical H^+ ion electro-adsorption/desorption region, a double layer charging current region, a Pt pre-oxidation region and a Pt reduction region. In the proton adsorption/desorption region, three peaks are easily observed at ca. −0.16, −0.085 and −0.025 V versus SCE. These are typical characteristic peaks for Pt (1 1 0), Pt (1 0 0) and Pt (1 1 1) for the polycrystalline Pt particles [23,24]. On the whole, the Pt/MCF-C-ETX shows high

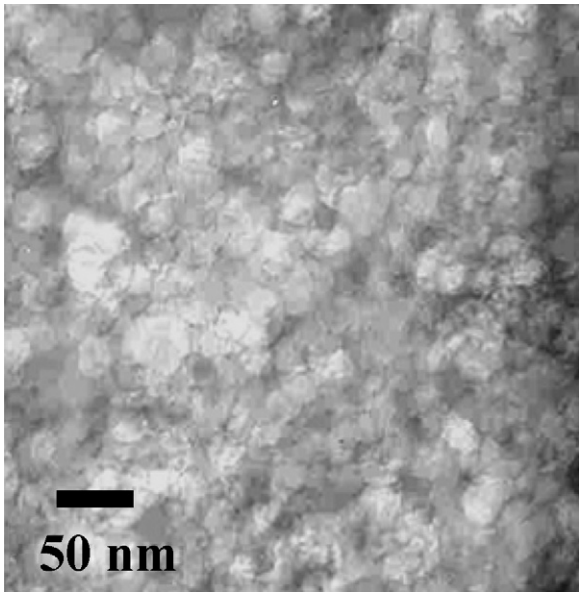

Fig. 4. TEM images of (a) MCF-C and (b) MCF-S.

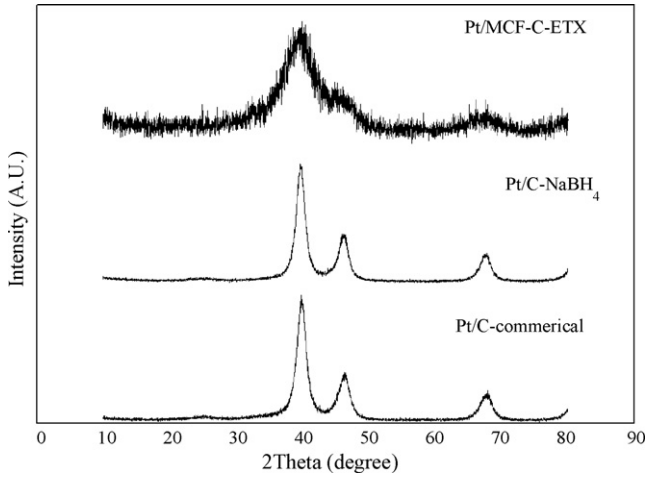

Fig. 5. XRD patterns of the prepared Pt catalysts.

Table 1
Average crystallite size calculated from Pt (2 2 0) using the Scherrer equation, surface area, EAS value by H^+ ion (S_{EAS-H}) adsorption and EAS value by CO adsorption (S_{EAS-CO})

	Particle size (nm)	Surface area (S_{Pt}) (m^2/g_{Pt})	S_{EAS-H} (m^2/g_{Pt})	S_{EAS-CO} (m^2/g_{Pt})
Pt/C-commercial	4.5	62	61	55
Pt/C-$NaBH_4$	4.6	60	59	52
Pt/MCF-C-ETX	2.5	112	95	84

double layer charging currents, which results from the high surface area of MCF-C. The peak area for the H^+ ion adosption/desorption current was used to estimate EAS values of supported Pt catalysts [25]. EAS values for the supported Pt catalysts were calculated from the integrated average charges for H^+ ion adsorption and desorption, corrected by eliminating the double layer charging current using the following equation:

$$S_{EAS-H} = \frac{Q_H}{0.21 \times [Pt]}$$

where S_{EAS-H}, Q_H, and [Pt] are the EAS (cm_2/g_{Pt}), the average columbic charge for hydrogen adsorption/desorption (C), and platinum loading (mg/cm^2), respectively. The value of 0.21 represents the charge density, required to oxidize a monolayer of H^+ ions on the Pt surface [26–30]. The calculation results are shown in Table 1. The EAS value for Pt/MCF-C-ETX is ca. 1.8 times larger than those of the other Pt catalysts, due to the high Pt dispersion. These results are in good agreement with trends obtained from TEM and an XRD analyses.

The Electrochemically active surface areas were further confirmed by CO stripping voltammetry. Representative CO stripping voltammograms for the Pt/C-commercial catalyst are shown in Fig. 8(a). After the adsorption of CO to the surface of Pt, the CO stripping peak appeared at ca. 0.455 V versus SCE, in the first cycle. A weak second peak and third peak also appeared at ca 0.507 and 0.546 V versus SCE. This indicates that the Pt/C-commercial catalyst is comprised of polycrystalline Pt nano-particles which have different activation sites for CO oxidation [23]. The CO stripping voltammograms for the supported Pt catalysts are shown in Fig. 8(b). Each of the supported Pt catalysts showed three peaks at different potentials, indicating the presence of polycrystalline Pt.

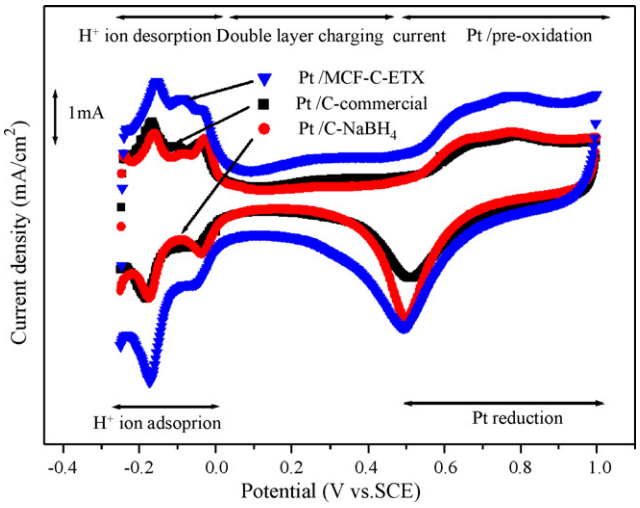

Fig. 7. Cyclic voltammograms (CVs) of the supported Pt catalysts under acidic electrolyte (0.5 M H_2SO_4).

To estimate EAS values using CO stripping voltammograms, a similar formula was employed. The charge Q_{CO} was used to calculate the electrochemically active surface area of the prepared Pt catalyst using the following equation:

$$S_{EAS-CO} = \frac{Q_{CO}}{0.484 \times [Pt]}$$

where the value of 0.484 represents the charge density required to oxidize a monolayer of CO on the Pt surface [23,26–30]. The S_{EAS-CO} values obtained by CO stripping voltammetry are listed in Table 1. It can be easily observed that the trends for S_{EAS-CO} were identical to those for S_{EAS-H} and surface area of Pt (S_{Pt}) determined from the XRD measurements. From the TEM, XRD and CVs data, it can be concluded that the Pt/MCF-C-ETX catalyst has the highest metal dispersion among the Pt catalysts employed in this work.

Fig. 9 shows cyclic voltammograms for methanol electro-oxidation for the supported Pt catalysts in a 0.5 M H_2SO_4 electrolyte solution containing 2 M CH_3OH at room temperature. The current for methanol electro-oxidation slowly increased between 0 and 0.4 V. The current steeply increased after 0.4 V and maximum peak current occurred at ca. 0.65 V. After the maximum peak current, it decreased because the

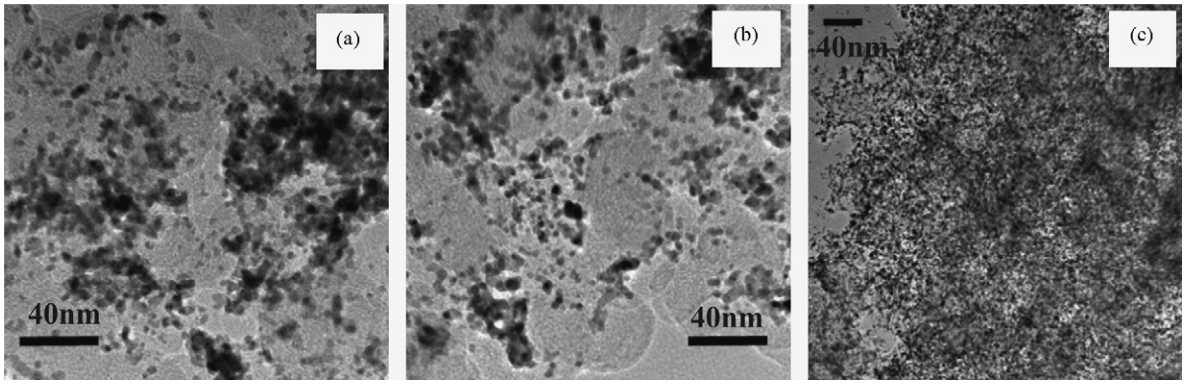

Fig. 6. TEM images of the prepared Pt catalyst: (a) Pt/C-commercial, (b) Pt/C-$NaBH_4$ and (c) Pt/MCF-C-ETX.

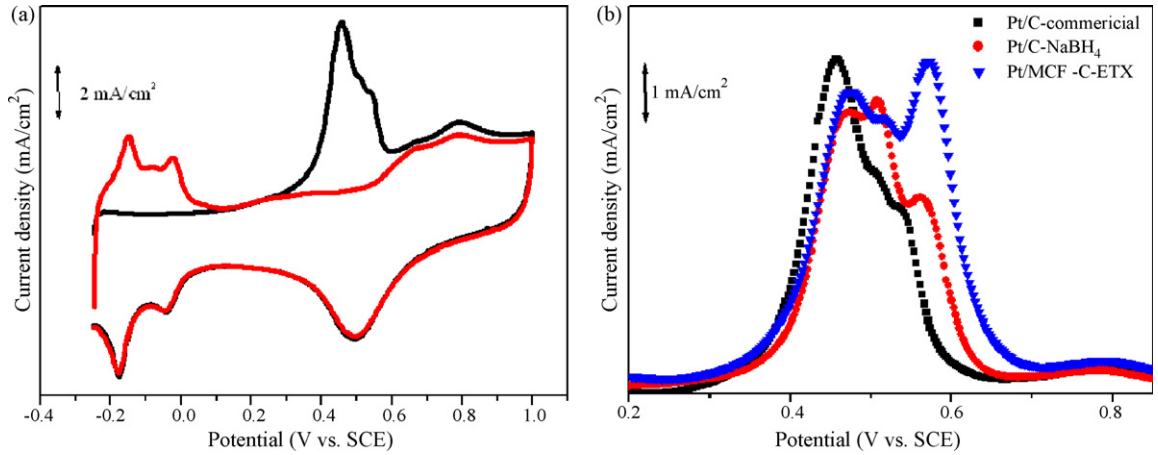

Fig. 8. (a) Representative CO stripping voltammograms of Pt/C-commercial catalysts and (b) CO stripping voltammograms of the supported Pt catalysts.

numbers of active sites for methanol electro-oxidation were decreased by the oxidation of active metal. After 0.8 V, the current re-increased, implying that methanol electro-oxidation occurred on surface of the Pt oxide. In a cathodic scan, the active sites were recovered due to the reduction of Pt oxide, to produce a methanol electro-oxidation current peak. In the CV for alcohol oxidation, current peaks are frequently used to compare catalytic activity.

It should be noted that the Pt/MCF-C-ETX catalyst exhibited the highest maximum current peaks among the supported Pt catalysts, indicating the superior catalytic activity for methanol electro-oxidation. As shown in the Fig. 9 insert image, the Pt/C-commercial catalyst showed a slightly higher oxidation peak than Pt/C-$NaBH_4$. Although the Pt/C-commercial showed a slightly higher current than Pt/C-$NaBH_4$, the Pt/C-$NaBH_4$ and Pt/C-commercial appeared to exhibit a similar catalytic activity for methanol electro-oxidation.

The Pt/MCF-C-ETX catalyst had the smallest Pt particles and the highest EAS value, which is related to active metal utilization. It is also thought that the pore structure of MCF-C is more beneficial on metal dispersion, compared to non-porous supports. In a practical fuel cell system, large pores are more desirable for distribution of bulky ionomer for the formation of a triple phase boundary and the facile diffusion of the reactants. In this work, the Pt/MCF-C-ETX showed the highest EAS value, which originated from the highest Pt dispersion and the smallest Pt size, resulting in the highest catalytic activity for methanol electro-oxidation. From the experimental results, it can be concluded that Pt/MCF-C-ETX is the most suitable not only in methanol electro-oxidation but also for a supported Pt catalyst as electrode materials in low-temperature fuel cells.

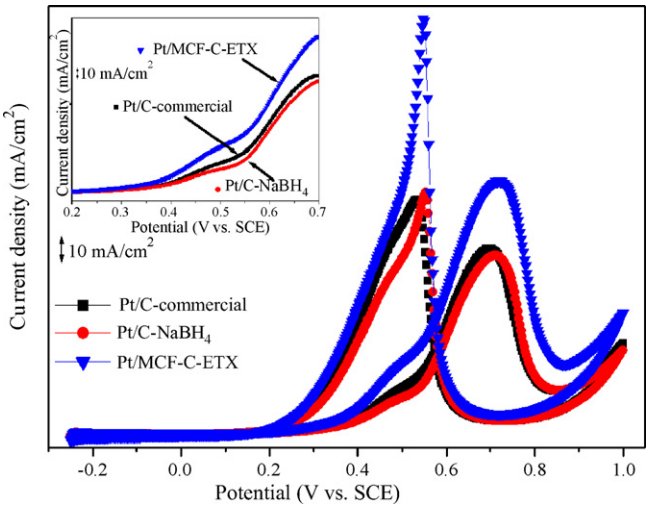

Fig. 9. Cyclic voltammograms of the supported Pt catalysts in 0.5 M H_2SO_4 containing 2 M CH_3OH.

4. Conclusions

In this work, a novel and simple preparation method for preparing MCF-C was proposed. Since the silica–polymer composites can be directly used for the preparation of the MCF-C, the process suggested in this work is very simple, economical and useful compared to conventional method. The prepared MCF-C was used as catalyst support for a Pt catalyst in methanol electro-oxidation. The Pt/MCF-C-ETX exhibited a smaller Pt particle size and a higher EAS value than other Pt catalysts employed in this work. In methanol electro-oxidation, the Pt/MCF-C-ETX showed the highest peak current, among the supported Pt catalysts. The highest catalytic performance is closely related to the high EAS value resulted from a high Pt dispersion.

Acknowledgement

Financial support for this research provided by the Hyundai-Kia Next Generation Vehicle Research Center is gratefully acknowledged.

References

[1] H. Li, S. Zhu, H. Xi, R. Wang, Microporous Mesoporous Mater. 89 (2006) 196.
[2] S. Yoon, J. Lee, T. Hyeon, S.M. Oh, J. Electrochem. Soc. 147 (2000) 2507.
[3] Y. Park, T. Kang, P. Kim, J. Lee, H. Kim, J. Yi, Catal. Today 97 (2004) 195.
[4] P.V. Samant, M.F.R. Pereira, J.L. Figueiredo, Catal. Today 102–103 (2005) 183.

[5] T. Kang, Y. Park, K. Choi, J.S. Lee, J. Yi, J. Mater. Chem. 14 (2004) 1043.
[6] H. Kim, P. Kim, J. Yi, K.Y. Lee, S.H. Yeom, I.K. Song, Stud. Surf. Sci. Catal. 159 (2006) 297.
[7] J. Lee, J. Kim, Y. Lee, S. Yoon, S.M. Oh, T. Hyeon, Chem. Mater. 16 (2004) 3323.
[8] S. Han, S. Kim, W. Choi, H. Park, J. Yoon, T. Hyeon, Microporous Mesoporous Mater. 58 (2003) 131.
[9] Y.M. Liu, W.L. Feng, T.C. Li, H.Y. He, W.L. Dai, W. Huang, Y. Cao, K.N. Fan, J. Catal. 239 (2006) 125.
[10] Q. Huo, R. Leon, P.M. Petroff, G.D. Stucky, Science 268 (1995) 1324.
[11] D. Zhao, J. Feng, Q. Huo, N. Melosh, G.H. Fredrickson, B.F. Chmelka, G.D. Stucky, Science 278 (1998) 548.
[12] J. Lee, J. Kim, S.W. Kim, C. Shin, T. Hyeon, Chem. Commun. (2004) 562.
[13] J. Lee, K. Sohn, T. Hyeon, J. Am. Chem. Soc. 131 (2001) 5146.
[14] W.W. Lukens, G.D. Stucky, Chem. Mater. 14 (2002) 1665.
[15] J. Lee, K. Sohn, T. Hyeon, Chem. Commun. (2002) 2674.
[16] P.V. Samant, J.B. Fernandes, C.M. Rangel, J.L. Figueiredo, Catal. Today 102–103 (2005) 173.
[17] J. Ding, K.Y. Chen, J. Ren, F. Xio, Electrochim. Acta 50 (2005) 3131.
[18] F. Su, X.S. Zhao, Y. Wang, J.Y. Lee, Microporous Mesoporous Mater. 98 (2007) 323.
[19] S. Joo, S. Choi, I.H. Oh, J. Kwak, Z. Liu, O. Terasaki, T. Ryoo, Nature 412 (2001) 169.
[20] P. Kim, J.B. Joo, W. Kim, J. Kim, I.K. Song, J. Yi, J. Mol. Catal. 263 (2007) 15.
[21] S. Mukerjee, S. Srinivasan, M.P. Soriaga, J. McReen, J. Electrochem. Soc. 142 (1995) 1409.
[22] C. Audo, J.F. Lambert, M. Che, B. Didillon, Catal. Today 65 (2001) 157.
[23] W. Vielstich, A. Lamm, H.A. Gasteiger, Handbook of Fuel Cells: Fundamentals Technology and Application, Wiley, 2003, pp. 368–391.
[24] J. Solla-Gullon, F.J. Vidal-Igalesias, E. Herrero, J.M. Feliu, A. Aldaz, Electrochem. Commun. 8 (2006) 189.
[25] A. Pozio, M. De Francesco, A. Cemmi, F. Cardellini, L. Giorgi, J. Power Sources 105 (2002) 13.
[26] J. Perez, E.R. Gonzalez, E.A. Ticianelli, Electrochim. Acta 44 (1998) 1329.
[27] G. Tamizhmani, J.P. Dodelet, D. Gury, J. Electrochem. Soc. 143 (1996) 18.
[28] J. Fournier, G. Faubert, J.Y. Tiquin, R. Cote, D. Guay, J.P. Dodelet, J. Electrochem. Soc. 144 (1997) 146.
[29] M. Ciureanu, H. Wang, J. Electrochem. Soc. 144 (1999) 4031.
[30] M.J. Weaver, S.C. Chang, L.W.H. Leung, X. Jiang, M. Rubel, M. Szkarczk, D. Zurawaki, A. Wieckowski, J. Electroanal. Chem. 327 (1992) 247.